arXiv:1606.06836v2 [cond-mat.str-el] 23 Jun 2016

From a quasimolecular band insulator to a relativistic Mott insulator in t_{2g}^5 systems with a honeycomb lattice structure

Beom Hyun Kim,[1,2] Tomonori Shirakawa,[3] and Seiji Yunoki[1,2,3,4]

[1] *Computational Condensed Matter Physics Laboratory, RIKEN, Wako, Saitama 351-0198, Japan*
[2] *Interdisciplinary Theoretical Science (iTHES) Research Group, RIKEN, Wako, Saitama 351-0198, Japan*
[3] *Computational Quantum Matter Research Team, RIKEN Center for Emergent Matter Science (CEMS), Wako, Saitama 351-0198, Japan*
[4] *Computational Materials Science Research Team, RIKEN Advanced Institute for Computational Science (AICS), Kobe, Hyogo 650-0047, Japan*

(Dated: March 14, 2019)

The t_{2g} orbitals of an edge-shared transition-metal oxide with a honeycomb lattice structure form dispersionless electronic bands when only hopping mediated by edge-shared oxygens is accessible. This is due to the formation of isolated quasimolecular orbitals (QMOs) in each hexagon, introduced recently by Mazin *et al.* [Phys. Rev. Lett. **109**, 197201 (2012)], which stabilizes a band insulating phase for t_{2g}^5 systems. However, the QMOs are fragile against the spin-orbit coupling (SOC) as well as the Coulomb repulsion. With help of the exact diagonalization method, we show that the electronic phase of t_{2g}^5 systems can vary from a quasimolecular band insulator to a relativistic $J_{\rm eff} = 1/2$ Mott insulator with increasing the SOC and Coulomb repulsion. The different electronic phases manifest themselves in electronic excitations observed in optical conductivity and resonant inelastic x-ray scattering. Based on our calculations, we assert that Ru^{3+}- and Ir^{4+}-based $4d$ and $5d$ transition-metal compounds are both far from quasimolecular band insulators.

PACS numbers: 71.10.-w,71.70.Ej,78.70.Ck,78.20.Bh

Introduction — Physical properties of $4d$ and $5d$ transition metal (TM) compounds with nominally less than six d electrons are determined by t_{2g} manifold because of strong cubic crystal field. Strong spin-orbit coupling (SOC) causes t_{2g} orbitals to be split into effective total angular momenta $j_{\rm eff} = 1/2$ and $3/2$. The relativistic electronic feature in these TM compounds has drawn much attraction recently as exotic electronic, magnetic, and topological phases have been expected, including $J_{\rm eff} = 1/2$ Mott insulator [1–5], superconductivity [6, 7], topological insulator [8, 9], Weyl semimetal [10, 11], and spin liquid [12, 13]. Among them, the research on t_{2g}^5 systems with edge-shared ligands forming a honeycomb lattice structure has been triggered by the possibility of a nontrivial topological phase [14, 15] or a Kitaev-type spin liquid [16–18], attributed to their unique hopping geometry. However, the existing compounds such as Na_2IrO_3 [19–22], Li_2IrO_3 [23], Li_2RhO_3 [24], and α-$RuCl_3$ [25–27], have been turned out to be magnetic insulators with a long-range antiferromagnic (AFM) or glassy-spin order.

In order to understand the electronic and magnetic structures of these compounds with t_{2g}^5 configuration, two distinct points of view, i.e., Mott- and Slater-type pictures, have been proposed. In the Mott picture, the Coulomb repulsion opens the gap of the relativistic $j_{\rm eff} = 1/2$ based band and the superexchange interaction between the relativistic isospins stabilizes the AFM order [28–30, 33, S5, S7]. This strong coupling approach can successfully elucidate the observed excitations in the optical conductivity (OC) and resonant inelastic x-ray scattering (RIXS) [S5]. However, there has been still debate on the origin of the zigzag AFM order in Na_2IrO_3 [34, 35]. In contrast, the Slater picture focuses on the itinerant nature of t_{2g} bands and treats the Coulomb interaction perturbatively. This weak coupling approach naturally explains the zigzag AFM order with a concomitantly induced band gap [36–39]. However, it is difficult to fully describe the observed excitations in the OC and RIXS of Na_2IrO_3 [40–42]. Because three relevant parameters, i.e., hopping integral, Coulomb repulsion, and SOC, are of similar energy scale, either of these two opposite pictures cannot be ruled out.

As the electron hoppings between the adjacent TMs via the two edge-sharing ligands are highly orbital dependent (see Fig. 1), the electron motion is confined within a single hexagon formed by six TMs. This has led to the notion of the quasimolecular orbital (QMO) formation introduced by Mazin *et al.* [36], where each t_{2g} orbital of a TM participates in the formation of QMOs at one of the three different hexagons around the TM. Therefore, when the SOC and Coulomb repulsion are both small, the ground state for t_{2g}^5 systems is a band insulator with a strong QMO character. However, when the SOC is strong, the QMOs are no longer well defined. This is because the SOC induces an effective hopping between neighboring QMOs. In this limit, the local relativistic $j_{\rm eff}$ orbitals are instead expected to play a dominant role in characterizing the electronic and magnetic structures.

In this paper, by considering a minimal microscopic model to capture both extreme limits, we examine the ground state phase diagram for t_{2g}^5 electron configuration with help of the numerically exact diagonalization method. We show that not only the SOC but also the

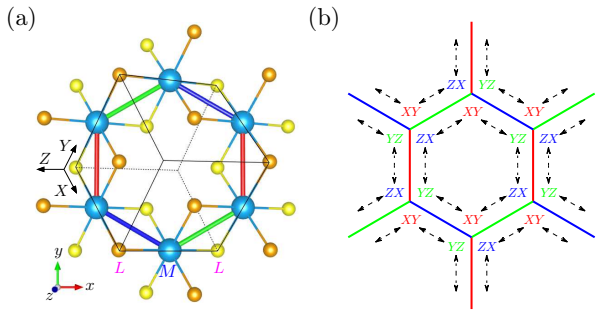

FIG. 1. (Color online) Schematic diagram of (a) a honeycomb lattice and (b) its accessible hopping mediated via edge-shared ligands. TMs (M) are denoted by clue spheres and ligands (L) above (blow) the hexagon formed by TMs are indicated by orange (yellow) spheres in (a). XY, YZ, and ZX in (b) refer to three t_{2g} orbitals (d_{XY}, d_{YZ}, and d_{ZX}, respectively), based on local coordinates (X, Y, and Z) indicated in (a). The global coordinates (x, y, and z) are also indicated in (a). The electron motion is bounded in each hexagon due to the bond-dependent hoppings when the SOC and Coulomb interaction are absent.

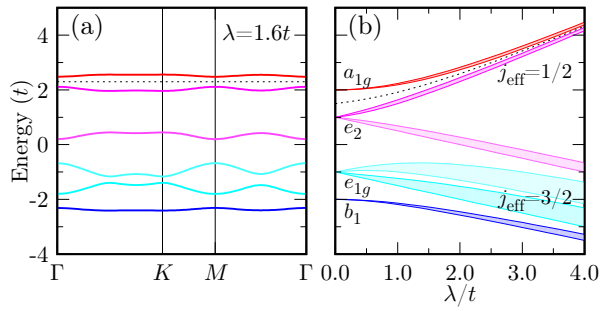

FIG. 2. (Color online) (a) Noninteracting band dispersion with the hopping $t\,(>0)$ mediated by edge-shared ligands for the SOC $\lambda = 1.6t$. Each band is doubly degenerate (Kramer's doublet). (b) Energy splitting of the noninteracting bands as a function of λ. Shade region represents the band width of each band. a_{1g}, e_{2u}, e_{1g}, and b_{1u} refer to the symmetries of the quasimolecular bands when $\lambda = 0$. Dotted lines denote the Fermi level for t_{2g}^5 systems.

Coulomb repulsion induces a crossover of the ground state with the strong QMO to relativistic $j_{\rm eff}$ orbital character. Concomitantly, the nature of the emerging electronic state varies from a quasimolecular band insulator to a relativistic $J_{\rm eff} = 1/2$ Mott insulator. The different electronic states are manifested in distinct behaviors of excitations, directly observed in OC and RIXS experiments. Our analysis concludes that Ru^{3+}- and Ir^{4+}-based systems are both far from the QMO state but rather the relativistic Mott insulator.

Noninteracting limit – Without the SOC, the QMOs are the exact eigenstates with b_{1u}, e_{1g}, e_{2u}, and a_{1g} symmetries, the eigenenergies being $-2t$, $-t$, t, and $2t$ (t: hopping between adjacent TMs), respectively [43], and they form dispersionless bands. However, as shown in Fig. 2(a), once the SOC λ is finite, the double degeneracy of e_{1g} and e_{2u} symmetries is lift and the QMOs are split in total into six Kramer's doublet bands with finite dispersion. With further increasing the SOC, the highest two bands as well as the lowest four bands come close in energy but the energy splitting between these two manifolds becomes larger, smoothly connecting to the $j_{\rm eff} = 1/2$ and $j_{\rm eff} = 3/2$ based bands [see Fig. 2(b)]. Thus, an insulating gap of t_{2g}^5 systems for $t > 0$ gradually decreases with continuous change of hole character from a_{1g} to $j_{\rm eff} = 1/2$ as λ increases.

Correlation effect — Let us now explore the effect of electron correlation by considering a three-band Hubbard model on a periodic six-site cluster, as shown in Fig. 1 [43], for electron density $n = 5$, with help of Lanczos exact diagonalization method [S1, S2]. We first examine the ground state as functions of the intra-orbital Coulomb repulsion U, Hund's coupling $J_{\rm H}$, and λ, and check the stability of the QMO state. For this purpose, we calculate the hole density $\bar{n}_{a_{1g}}$ of the a_{1g} quasimolecular band at the Γ point, which is exactly one for the pure QMO state [43]. Figure 3(a) shows the results of $\bar{n}_{a_{1g}}$ with varying U and λ when $J_{\rm H} = 0$. The strong SOC mixes the three t_{2g} orbital at each site, which gives rise to a finite overlap between QMOs in neighboring hexagons. The Coulomb interaction is also adequate to promote the scattering among electrons bounded in adjacent hexagons. Therefore, as shown in Fig. 3(a), λ and U are both destructive perturbations to the QMOs.

The ground state is described by a direct product of local states with not only d^5 electron configuration but also other configurations such as d^4 and d^6. Therefore, the ground state is sensitive to the local multiplet structures of these electron configurations. According to the multiplet theory, the Hund's coupling $J_{\rm H}$ always brings about additional splitting of the d^4 multiplet hierarchy [43]. It is thus easily conjectured that $J_{\rm H}$ also plays a role in the QMO formation. Figure 3(b) well represents the effect of $J_{\rm H}$ on the QMO state. In finite $J_{\rm H}$, the region with the strong QMO character shrinks with reduced $\bar{n}_{a_{1g}}$ and the crossover boundary becomes sharper.

In the whole parameter region of Fig. 3, the ground state is insulating. However, it is legitimate to expect that the insulating nature is varied from a band insulator to a Mott insulator across the boundary where the QMO character is abruptly lost. To verify this conjecture, we calculate the excitation spectrum $\Lambda_{1/2}(\omega)$ of a doublon-holon pair formed in the $j_{\rm eff} = 1/2$ orbitals at neighboring sites [43], excitations schematically shown in 'B' of Fig. 4(j), which directly gives the charge gap structure. As shown in Figs. 4(a)–(c), the U dependence of $\Lambda_{1/2}(\omega)$ is qualitatively different across the crossover boundary. Before the boundary where the QMO character is strong, the low energy excitations shift downward in spite of increasing U, implying that an insulating gap

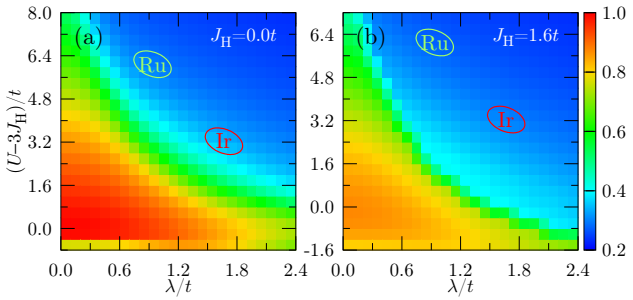

FIG. 3. (Color online) The hole density $\bar{n}_{a_{1g}}$ of the a_{1g} quasimolecular band at the Γ point as functions of U and λ for (a) $J_H = 0$ and (b) $J_H = 1.6t$. Note that $\bar{n}_{a_{1g}} = 1$ for the pure QMO state. The loci of Ru^{3+}- and Ir^{4+}-based $4d$ and $5d$ transition-metal compounds are also indicated.

evidently decreases with increasing the electron correlation. In contrast, after the boundary where the QMO character is lost, the clear increase of the lowest peak position is manifested with increasing U, indicating the increase of the gap as in a Mott insulator. The similar feature is also found when λ is increased with fixed U and J_H [43]. These results support the conjecture that the insulating nature changes across the crossover boundary. As shown in the following, the conjecture is further supported by other excitation spectra.

OC and RIXS spectra — The Kubo formula and the continued fraction method are exploited to investigate the OC and L_3-edge RIXS spectra [43]. Figures 4(d)–(i) summarize the results for $\lambda = 0.6t$, $0.8t$, and $1.6t$ with J_H=$1.6t$. Note that the QMO character suddenly diminishes at $U-3J_H \sim 3t$ for $\lambda = 0.6t$, $2t$ for $0.8t$, and 0 for $1.6t$, as shown in Fig. 3(b). The abrupt change of the electronic characteristics is reflected in these excitation spectra.

When the QMO character is strong with large $\bar{n}_{a_{1g}}$, the OC exhibits two-peak and three-peak structures for $\lambda = 0.6t$ and $0.8t$, and $1.6t$, respectively. The lower (higher) peak in the OC is attributed to the transition between the a_{1g} and e_{2u} (e_{1g}) quasimolecular bands whose energies are around t ($3t$) (see Fig. 2). The large splitting of the e_{2u} bands for the strong SOC can give an additional splitting to the lower peak in the OC. The RIXS spectra also shows the similar peak structures near the similar excitation energies. Consequently, the excitations can be interpreted on the basis of the single-particle picture. Therefore, a strong band insulating character is predominant in this region.

In the region where the QMO character is degraded, the OC shows a one-peak structure and the peak position monotonically increases with U, while the RIXS spectra exhibits the dominant peak around $3\lambda/2$ in addition to an almost zero energy peak due to the magnetic excitation. These features can be well understood as on-site or inter-site electron-hole excitations in the local relativistic $j_{\rm eff}$ orbitals. As shown in 'B' and 'C' of Fig. 4(j), two types of inter-site electron-hole excitations can play a role in the OC. However, the edge-shared geometry suppresses the contribution of type 'B' electron-hole excitation simply because the hopping between the neighboring $j_{\rm eff} = 1/2$ orbitals is zero [46]. Hence, only type 'C' electron-hole excitation gives the dominant contribution to form the one-peak like structure at excitation energy $\omega \approx U - 3J_H + \frac{3\lambda}{2}$. In the RIXS spectra, an on-site electron-hole excitation indicated in 'A' of Fig. 4(j), i.e., a local d-d transition between the $j_{\rm eff} = 3/2$ and $j_{\rm eff} = 1/2$ orbitals, can give a dominant intensity at $\omega \approx 3\lambda/2$. Thus, both OC and RIXS spectra in this region can be interpreted in terms of the relativistic Mott insulating picture.

In the relativistic Mott insulator limit, the RIXS spectra show an additional peak below the local d-d excitation ($\approx 3\lambda/2$) and above the almost zero energy magnetic peak, which is marked by triangles in Figs. 4(g)–(i). Indeed, this peak has been observed in Na_2IrO_3 and the origin is attributed to the exciton formation induced by the inter-site electron correlation [29]. However, the consecutive theoretical study has verified that this exciton-like peak appears even without considering the inter-site electron correlation when the inter-site migration of electrons from the $j_{\rm eff} = 1/2$ to $3/2$ orbitals ['B' of Fig. 4(j)] follows the local d-d transition ['A' of Fig. 4(j)], resulting in the inter-site electron-hole excitation between the $j_{\rm eff} = 1/2$ orbitals [S5]. The excitation spectrum $\Lambda_{1/2}(\omega)$ of a doublon-holon pair in the $j_{\rm eff} = 1/2$ orbitals shown in Figs. 4(a)–(c) also yield the obvious spectral weight in the vicinity of the exciton-like RIXS excitation energy, implying that these excitations are due to the same origin. In addition, the monotonic increase of the exciton-like peak position in the RIXS with U is also consistent with $\Lambda_{1/2}(\omega)$. Thus, it is reasonable to infer that the origin of the exciton-like peak near the edge of local d-d excitation in the RIXS is due to the combined excitations of two different types ('A' and 'B').

Ir^{4+}- and Ru^{3+}-based systems — A typical SOC is known to be 0.4–0.5 eV for $5d$ systems and 0.1–0.2 eV for $4d$ systems [47, 48]. Recent theoretical studies have estimated that $t \approx 0.27$ eV for the most studied Ir^{4+} system Na_2IrO_3 [36, 38, 49], and $t \approx 0.11$ eV [33] and 0.16 eV [S6] for α-$RuCl_3$ (Ru^{3+}), both of which are much smaller than that for Ir^{4+} systems. U and J_H, however, are not easy to be determined because the full screening effect of electron correlation is hardly treated. One useful expedient is to extract them from the OC measurement.

As discussed above, the dominant optical peak appears near $U-3J_H+\frac{3\lambda}{2}$. Thus, we can estimate $U-3J_H \sim 0.8$–1.0 eV for Na_2IrO_3 based on the existing OC data, which exhibits a one-peak structure around 1.6 eV [28, 30]. Assuming $U-3J_H = 3.2t$ (≈ 0.86 eV), our results for the OC and RIXS spectra in Figs. 4(f) and (i) are both indeed in good quantitative agreement with the experiments [28–30], except for a double-peak structure around 0.7 eV

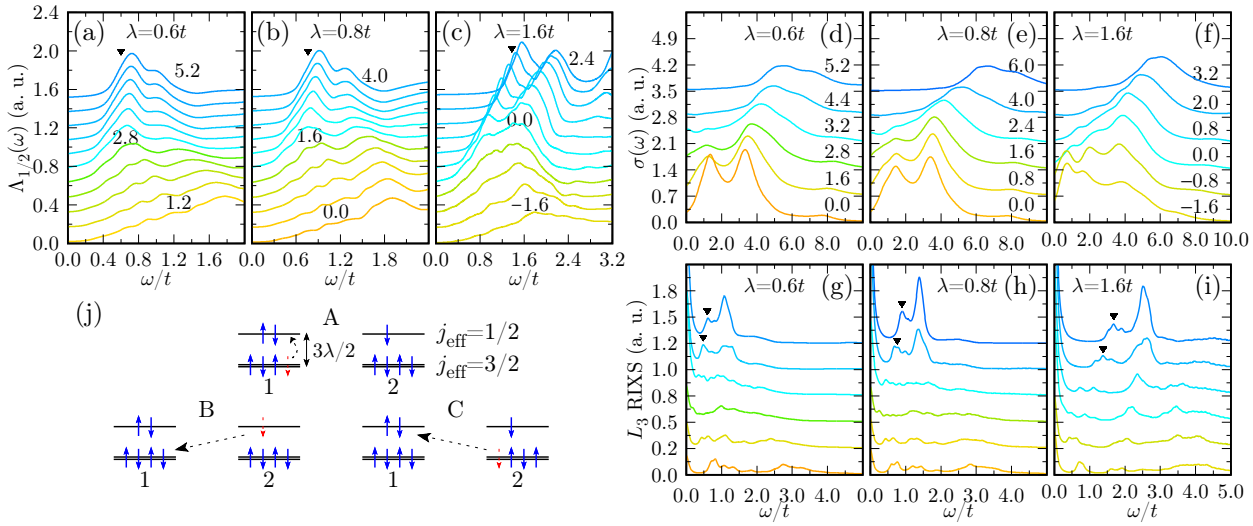

FIG. 4. (Color online) (a)–(c): Excitation spectrum $\Lambda_{1/2}(\omega)$ of a doublon-holon pair formed in the neighboring $j_{\rm eff} = 1/2$ orbitals for (a) $\lambda = 0.6t$, (b) $0.8t$, and (c) $1.6t$ with various $(U - 3J_{\rm H})/t$ values (the same increment of $0.4t$) indicated in the figures. (d)–(i): OC $\sigma(\omega)$ and L_3-edge RIXS spectra at wave number $\mathbf{q} = 0$ for $\lambda = 0.6t$ [(d) and (g)], $0.8t$ [(e) and (h)], and $1.6t$ [(f) and (i)] with various values of $(U - 3J_{\rm H})/t$ indicated in the figures. We set $J_{\rm H} = 1.6t$ and different line colors correspond to the values of $\bar{n}_{a_{1g}}$ shown in Fig. 3(b). The exciton-like excitations in the RIXS are indicated by solid triangles in (g)–(i), and the corresponding peak positions are also indicated in (a), (b), and (c) for $U - 3J_{\rm H} = 5.2t$, $4t$, and $2t$ respectively. (j) Schematic energy diagrams of three relevant electron-hole excitations. Blue solid and red dotted arrows refer to electron and hole, respectively, with up or down spin. "1" and "2" indicate two neighboring metal sites.

($\approx 2.6t$) observed in the RIXS experiment, instead of a single peak found in Fig. 4(i). However, it is well known that the additional trigonal distortion splits the single peak into the double peaks [29, S5]. Therefore, we can conclude that the electronic state of Na_2IrO_3 is far from the QMO limit and is located in the relativistic Mott insulating region, as indicated in Fig. 3.

The recent optical absorption experiments for α-$RuCl_3$ have found a dominant peak around 1.2 eV as well as a small additional peak near 0.3 eV [S7, S8]. The photoemission spectroscopy measurement has also observed a large gap about 1.2 eV [52]. Thus, $U - 3J_{\rm H}$ for α-$RuCl_3$ is estimated to be about 0.9–1.1 eV. If we adopt $t = 0.16$ eV, our result for $U - 3J_{\rm H} = 6t$ (≈ 0.96 eV) and $\lambda = 0.8t$ (≈ 0.13 eV) in Fig. 4(e) also exhibits the dominant peak near 1.1 eV ($\approx 6.9t$). Although no experimental RIXS spectrum has been reported yet, recent neutron scattering measurement on α-$RuCl_3$ observed an inelastic peak near 195 meV and estimated that $\lambda \approx 130$ meV [53]. This observation is consistent with a dominant RIXS peak around $1.4t$ (≈ 0.22 eV) for $U - 3J_{\rm H} = 6t$ in Fig. 4(h). Therefore, we expect that α-$RuCl_3$ is located also in the QMO poor region, as indicated in Fig. 3.

It should be noted, however, that the OC for $U - 3J_{\rm H} = 6t$ in Fig. 4(e) fails to yield the low-energy peak near 0.3 eV observed experimentally in α-$RuCl_3$. This can be explained by considering an additional direct d-d hopping t' between neighboring sites, estimated as large as -0.23 eV in Ref. 33 and -0.15 eV in Ref. S6. As discussed in Supplemental Material [43], the low-energy peaks attributed to the local d-d transition ['A' in Fig. 4(j)] can emerge because the forbidden optical transition among the $j_{\rm eff} = 1/2$ bands can be accessed due to the direct hopping t' [54]. The experimental fact that the intensity of the low-energy peak near 0.3 eV is much weaker than that of the dominant peak around 1.2 eV suggests that the strength of t' is not as large as the previous theoretical expectations [43].

Conclusion — Based on the numerically exact diagonalization analyses of the three-band Hubbard model, we have shown that the ground state of the t_{2g}^5 system with the honeycomb lattice structure can be transferred from a quasimolecular band insulator to a relativistic Mott insulator with increasing U and λ when the QMOs are disturbed and eventually replaced by the local relativistic $j_{\rm eff}$ orbitals. We have demonstrated that the different electronic nature of these insulators is manifested in the electronic excitations observed in OC and RIXS. Comparing our results with experiments, we predict that not only Na_2IrO_3 with strong SOC but also α-$RuCl_3$ with moderate SOC is the relativistic Mott insulator. This deserves further experimental confirmation, especially for α-$RuCl_3$ where we expect the exciton-like excitation near the edge of the local d-d excitation in the RIXS spectrum.

Acknowledgements — The numerical computations have been performed with the RIKEN supercomputer system (HOKUSAI GreatWave). This work has been supported by Grant-in-Aid for Scientific Research from MEXT Japan under the Grant No. 25287096 and also by RIKEN iTHES Project and Molecular Systems.

[1] B. J. Kim, H. Jin, S. J. Moon, J.-Y. Kim, B.-G. Park, C. S. Leem, J. Yu, T. W. Noh, C. Kim, S.-J. Oh, J.-H. Park, V. Durairaj, G. Cao, and E. Rotenberg, Phys. Rev. Lett. **101**, 076402 (2008).

[2] B. J. Kim, H. Ohsumi, T. Komesu, S. Sakai, T. Morita, H. Takagi, and T. Arima, Science **323**, 1329 (2009).

[3] G. Jackeli and G. Khaliullin, Phys. Rev. Lett. 102, 017205 (2009).

[4] H. Watanabe, T. Shirakawa, and S. Yunoki, Phys. Rev. Lett. **105**, 216410 (2010).

[5] C. Martins, M. Aichhorn, L. Vaugier, and S. Biermann, Phys. Rev. Lett. **107**, 266404 (2011).

[6] F. Wang and T. Senthil, Phys. Rev. Lett. **106**, 136402 (2011).

[7] H. Watanabe, T. Shirakawa, and S. Yunoki, Phys. Rev. Lett. **110**, 027002 (2013).

[8] D. Pesin and L. Balents, Nature Phys. **6**, 376 (2010).

[9] B.-J. Yang and Y. B. Kim, Phys. Rev. B **82**, 085111 (2010).

[10] W. Witczak-Krempa and Y. B. Kim, Phys. Rev. B **85**, 045124 (2012).

[11] A. Go, W. Witczak-Krempa, G. S. Jeon, K. Park, and Y. B. Kim, Phys. Rev. Lett. **109**, 066401 (2012).

[12] Y. Okamoto, M. Nohara, H. Aruga-Katori, and H. Takagi, Phys. Rev. Lett. **99**, 137207 (2007).

[13] Y. Singh, Y. Tokiwa, J. dong, and P. Gegenwart, Phys. Rev. B **88**, 220413(R) (2013).

[14] A. Shitade, H. Katsura, J. Kuneš, X.-L. Qi, S.-C. Zhang, and N. Nagaosa, Phys. Rev. Lett. **102**, 256403 (2009).

[15] C. H. Kim, H. S. Kim, H. Jeong, H. Jin, and J. Yu, Phys. Rev. Lett. **108**, 106401 (2012).

[16] J. Chaloupka, G. Jackeli, and G. Khaliullin, Phys. Rev. Lett. **105**, 027204 (2010).

[17] H.-C. Jiang, Z.-C. Gu, X.-L. Qi, and S. Trebst, Phys. Rev. B **83**, 245104 (2011).

[18] J. Reuther, R. Thomale, and S. Trebst, Phys. Rev. B **84**, 100406(R) (2011).

[19] Y. Singh and P. Gegenwart, Phys. Rev. B **82**, 064412 (2010).

[20] X. Liu, T. Berlijn, W.-G. Yin, W. Ku, A. Tsvelik, Y.-J. Kim, H. Gretarsson, Y. Singh, P. Gegenwart, and J. P. Hill, Phys. Rev. B **83**, 220403(R) (2011).

[21] S. K. Choi, R. Coldea, A. N. Kolmogorov, T. Lancaster, I. I. Mazin, S. J. Blundell, P. G. Radaelli, Y. Singh, P. Gegenwart, K. R. Choi, S.-W. Cheong, P.J. Baker, C. Stock, and J. Taylor, Phys. Rev. Lett. **108**, 127204 (2012).

[22] F. Ye, S. Chi, H. Cao, B. C. Chakoumakos, J. A. Fernandez-Baca, R. Custelcean, T. F. Qi, O. B. Korneta, and G. Cao, Phys. Rev. B **85**, 180403(R) (2012).

[23] Y. Singh, S. Manni, J. Reuther, T. Berlijn, R. Thomale, W. Ku, S. Trebst, and P. Gegenwart, Phys. Rev. Lett. **108**, 127203 (2012).

[24] Y. Luo, C. Cao, B. Si, Y. Li, J. Bao, H. Guo, X. Yang, C. Shen, C. Feng, J. Dai, G. Cao, and Z.-a. Xu, Phys. Rev. B **87**, 161121(R) (2013).

[25] J. A. Sears, M. Songvilay, K. W. Plumb, J. P. Clancy, Y. Qiu, Y. Zhao, D. Parshall, and Y.-J. Kim, Phys. Rev B **91**, 144420 (2015).

[26] M. Majumder, M. Schmidt, H. Rosner, A. A. Tsirlin, H. Yasuoka, and M. Baenitz, Phys. Rev B **91**, 180401(R) (2015).

[27] R. D. Johnson, S. C. Williams, A. A. Haghighirad, J. Singleton, V. Zapf, P. Manuel, I. I. Mazin, Y. Li, H. O. Jeschke, R. Valentí, and R. Coldea, Phys. Rev. B **92**, 235119 (2015).

[28] R. Comin, G. Levy, B. Ludbrook, Z.-H. Zhu, C. N. Veenstra, J. A. Rosen, Y. Singh, P. Gegenwart, D. Stricker, J. N. Hancock, D. van der Marel, I. S. Elfimov, and A. Damascelli, Phys. Rev. Lett. **109**, 266406 (2012).

[29] H. Gretarsson, J. P. Clancy, X. Liu, J. P. Hill, E. Bozin, Y. Singh, S. Manni, P. Gegenwart, J. Kim, A. H. Said, D. Casa, T. Gog, M. H. Upton, H.-S. Kim, J. Yu, V. M. Katukuri, L. Hozoi, J. van den Brink, and Y.-J. Kim, Phys. Rev. Lett **110**, 076402 (2013).

[30] C. H. Sohn, H.-S. Kim, T. F. Qi, D. W. Jeong, H. J. Park, H. K. Yoo, H. H. Kim, J.-Y. Kim, T. D. Kang, D.-Y. Cho, G. Cao, J. Yu, S. J. Moon, and T. W. Noh, Phys. Rev. B **88**, 085125 (2013).

[31] B. H. Kim, G. Khaliullin, and B. I. Min, Phys. Rev. B **89**, 081109(R) (2014).

[32] K. W. Plumb, J. P. Clancy, L. J. Sandilands, V. V. Shankar, Y. F. Hu, K. S. Burch, H.-Y. Kee, and Y.-J. Kim, Phys. Rev. B **90**, 041112(R) (2014).

[33] H.-S. Kim, V. Shankar V., A. Catuneanu, and H.-Y. Kee, Phys. Rev. B **91**, 241110(R) (2015).

[34] I. Kimchi and Y.-Z. You, Phys. Rev. B **84**, 180407(R) (2011).

[35] J. Chaloupka, G. Jackeli, and G. Khaliullin, Phys. Rev. Lett. **110**, 097204 (2013).

[36] I. I. Mazin, H. O. Jeschek, K. Foyevtsova, R. Valentí, and D. I. Khomskii, Phys. Rev. Lett. **109**, 197201 (2012).

[37] I. I. Mazin, S. Manni, K. Foyevtsova, H. O. Jeschke, P. Gegenwart, and R. Valentí, Phys. Rev. B **88**, 035115 (2013).

[38] K. Foyevtsova, H. O. Jeschke, I. I. Mazin, D. I. Khomskii, and R. Valentí, Phys. Rev. B **88**, 035107 (2013).

[39] H.-J. Kim, J.-H. Lee, and J.-H. Cho, Sci. Rep. **4**, 5253 (2014).

[40] Y. Li, K. Foyevtsova, H. O. Jeschke, and R. Valentí, Phys. Rev. B **91**, 161101(R) (2014).

[41] M. Kim, B. H. Kim, and B. I. Min, Phys. Rev. B **93**, 195135 (2016).

[42] J.-i. Igarashi and T. Nagao, J. Phys.: Condens. Matter **28**, 026006 (2016).

[43] See Supplemental Material for the detailed Hamiltonian, quasimolecular bands, cluster calculation of $\bar{n}_{a_{1g}}$, $\Lambda_{1/2}(\omega)$, OC and RIXS spectra, local multiplet structures, and the effect of the direct hopping on OC and RIXS spectra.

[44] R. B. Morgan and D. S. Scott, SIAM J. Sci. Comput. **14**, 585 (1993).

[45] E. Dagotto, Rev. Mod. Phys. **66**, 763 (1994).

[46] Let t and t' be the nearest neighbor hoppings between YZ and ZX orbitals, and between XY orbitals, respectively, along the XY-direction. One can show that the nearest neighbor hopping between $j_{\rm eff} = 1/2$ orbitals with the same isospin is $t'/3$. Therefore, there is no optical transition among the pure $j_{\rm eff} = 1/2$ bands without t'.

[47] D. Dai, H. J. Xiang, and M.-H. Whangbo, J. Comput. Chem. **29**, 2187 (2008).

[48] J. P. Clancy, N. Chen, C. Y. Kim, W. F. Chen, K. W. Plumb, B. C. Jeon, T. W. Noh, and Y.-J. Kim, Phys. Rev. B **86**, 195131 (2012).

[49] Y. Yamaji, Y. Nomura, M. Kurita, R. Arita, and M. Imada, Phys. Rev. Lett. **113**, 107201 (2014).

[50] S. M. Winter, Y. Li, H. O. Jeschke, and R. Valentí,

arXiv:1603.02548.
[51] L. J. Sandilands, Y. Tian, A. A. Reijnders, H.-S. Kim, K. W. Plumb, Y.-J. Kim, H.-Y. Kee, and K. S. Burch, Phys. Rev. B **93**, 075144 (2016).
[52] A. Koitzsch, C. Habenicht, E. Mueller, M. Knupfer, B. Buechner, H. Kandpal, J. van den Brink, D. Nowak, A. Isaeva, and Th. Doert, arXiv:1603.05507.
[53] A. Banerjee, C. A. Bridges, J.-Q. Yan, A. A. Aczel, L. Li, M. B. Stone, G. E. Granroth, M. D. Lumsden, Y. Yiu, J. Knolle, S. Bhattacharjee, D. L. Kovrizhin, R. Moessner, D. A. Tennant, D. G. Mandrus, and S. E. Nagler, DOI:10.1038/nmat4604.
[54] In Ref. S8, the small low-energy peak near 0.3 eV is attributed to an optically forbidden local d-d transition from the t_{2g} bands to the e_g bands through electron-phonon coupling. However, our result supports that the pure electronic transition within the t_{2g} manifold can give rise to the low-energy optical excitations.

Supplementary Materials
From a quasimolecular band insulator to a relativistic Mott insulator in t_{2g}^5 systems with a honeycomb lattice structure

HAMILTONIAN

We adopt the following three-band Hubbard Hamiltonian

$$H = \sum_{i,\delta,\mu,\nu,\sigma} t^{\delta}_{\mu\nu} c^{\dagger}_{i_\delta\mu\sigma} c_{i\nu\sigma} + \lambda \sum_{i,\mu,\nu,\sigma,\sigma'} (\mathbf{l}\cdot\mathbf{s})_{\mu\sigma,\nu\sigma'} c^{\dagger}_{i\mu\sigma} c_{i\nu\sigma'}$$
$$+ \frac{1}{2} \sum_{i,\sigma,\sigma',\mu,\nu} U_{\mu\nu} c^{\dagger}_{i\mu\sigma} c^{\dagger}_{i\nu\sigma'} c_{i\nu\sigma'} c_{i\mu\sigma} + \frac{1}{2} \sum_{\substack{i,\sigma,\sigma',\mu,\nu \\ (\mu\neq\nu)}} J_{\mu\nu} c^{\dagger}_{i\mu\sigma} c^{\dagger}_{i\nu\sigma'} c_{i\mu\sigma'} c_{i\nu\sigma} + \frac{1}{2} \sum_{\substack{i,\sigma,\mu,\nu \\ (\mu\neq\nu)}} J'_{\mu\nu} c^{\dagger}_{i\mu\sigma} c^{\dagger}_{i\mu\bar{\sigma}} c_{i\nu\bar{\sigma}} c_{i\nu\sigma}, \quad (1)$$

where $c^{\dagger}_{i\nu\sigma}$ is the creation operator of an electron with orbital $\nu\,(= XY, YZ, ZX)$ and spin $\sigma\,(=\uparrow,\downarrow)$ at site i in the honeycomb lattice, and three t_{2g} orbitals XY, YZ, and ZX correspond respectively to d_{XY}, d_{YZ}, and d_{ZX} orbitals defined in the local octahedron coordinates (X, Y, and Z), as indicated in Fig. 1(a) of the main text. δ in the first term denotes the three nearest neighboring (NN) directions in the honeycomb lattice and i_δ is the δ-directional NN site from site i. $\bar{\sigma}$ stands for the opposite spin of σ. The NN hopping matrix $t^{\delta}_{\mu\nu}$ is given in table S1. We assume the Kanamori-type Coulomb interaction, i.e., $U_{\mu\mu} = U$, $U_{\mu\neq\nu} = U - 2J_{\rm H}$, and $J_{\mu\nu} = J'_{\mu\nu} = J_{\rm H}$.

Let us define the local orbitals $\tilde{y}$, $\tilde{z}$, and $\tilde{x}$ in the global coordinates (x, y, and z) of the honeycomb lattice [see Fig. 1(a)]:

$$|\tilde{y}\rangle = \frac{1}{\sqrt{2}} \left(|ZX\rangle - |YZ\rangle \right), \quad (2)$$

$$|\tilde{z}\rangle = \frac{1}{\sqrt{3}} \left(|ZX\rangle + |XY\rangle + |YZ\rangle \right), \quad (3)$$

$$|\tilde{x}\rangle = \frac{1}{\sqrt{6}} \left(|ZX\rangle - 2|XY\rangle + |YZ\rangle \right). \quad (4)$$

Notice that the unitary transformation above from ZX, XY, and YZ orbitals to $\tilde{y}$, $\tilde{z}$, and $\tilde{x}$ orbitals is exactly the same as that for p orbitals from p_Y, p_Z, and p_X orbitals in the local coordinates to p_y, p_z, and p_x orbitals in the global coordinates. With these orbitals as the basis set, the spin-orbit coupling (SOC) is nonzero only for $\langle \tilde{x}\sigma|\mathbf{l}\cdot\mathbf{s}|\tilde{y}\sigma\rangle = \frac{i}{2} s_\sigma$,

TABLE S1. Hopping matrix $t^{\delta}_{\mu\nu}$ along three different directions. The XY-, YZ-, and ZX-directions refer to the bond directions between nearest neighboring transition metals where the two edge-sharing ligands connecting these metals are located in the XY-, YZ-, and ZX-planes, respectively (see Fig. 1).

XY-direction				YZ-direction				ZX-direction			
	$\|ZX\rangle$	$\|XY\rangle$	$\|YZ\rangle$		$\|ZX\rangle$	$\|XY\rangle$	$\|YZ\rangle$		$\|ZX\rangle$	$\|XY\rangle$	$\|YZ\rangle$
$\langle ZX\|$	0	0	t	$\langle ZX\|$	0	t	0	$\langle ZX\|$	0	0	0
$\langle XY\|$	0	0	0	$\langle XY\|$	t	0	0	$\langle XY\|$	0	0	t
$\langle YZ\|$	t	0	0	$\langle YZ\|$	0	0	0	$\langle YZ\|$	0	t	0

$\langle\tilde{y}\sigma|\mathbf{l}\cdot\mathbf{s}|\tilde{z}\bar{\sigma}\rangle = \frac{i}{2}$, and $\langle\tilde{z}\sigma|\mathbf{l}\cdot\mathbf{s}|\tilde{x}\bar{\sigma}\rangle = \frac{1}{2}s_\sigma$, where $s_\sigma = 1\,(-1)$ for $\sigma =\uparrow\ (\downarrow)$ and the imaginary unit i should not be confused with the site index i in Eq. (1). The local SOC term can be readily diagonalized in terms of the relativistic orbitals with the effective total angular momentum $j_{\rm eff} = 1/2$, i.e.,

$$|j_{\rm eff} = 1/2, j^z_{\rm eff} = +1/2\rangle = -\frac{1}{\sqrt{3}}\left(|\tilde{z}+\rangle + |\tilde{x}-\rangle + i|\tilde{y}-\rangle\right), \tag{5}$$

$$|j_{\rm eff} = 1/2, j^z_{\rm eff} = -1/2\rangle = +\frac{1}{\sqrt{3}}\left(|\tilde{z}-\rangle - |\tilde{x}+\rangle + i|\tilde{y}+\rangle\right), \tag{6}$$

and those with $j_{\rm eff} = 3/2$, i.e.,

$$|j_{\rm eff} = 3/2, j^z_{\rm eff} = +3/2\rangle = -\frac{1}{\sqrt{2}}\left(|\tilde{x}+\rangle + i|\tilde{y}+\rangle\right), \tag{7}$$

$$|j_{\rm eff} = 3/2, j^z_{\rm eff} = +1/2\rangle = +\frac{1}{\sqrt{6}}\left(2|\tilde{z}+\rangle - |\tilde{x}-\rangle - i|\tilde{y}-\rangle\right), \tag{8}$$

$$|j_{\rm eff} = 3/2, j^z_{\rm eff} = -1/2\rangle = +\frac{1}{\sqrt{6}}\left(2|\tilde{z}-\rangle + |\tilde{x}+\rangle - i|\tilde{y}+\rangle\right), \tag{9}$$

$$|j_{\rm eff} = 3/2, j^z_{\rm eff} = -3/2\rangle = +\frac{1}{\sqrt{2}}\left(|\tilde{x}-\rangle - i|\tilde{y}-\rangle\right), \tag{10}$$

whose energies are $\lambda/2$ for $j_{\rm eff} = 1/2$ and $-\lambda$ for $j_{\rm eff} = 3/2$.

QUASIMOLECULAR BANDS

Let us define the unit lattice vectors $\vec{a}_1 = \sqrt{3}a\hat{x}$ and $\vec{a}_2 = -\frac{\sqrt{3}a}{2}\hat{x} + \frac{3a}{2}\hat{y}$ of the honeycomb lattice (see Fig. S1), where a is the lattice constant between NN sites. Note that the unit cell contains two basis sites, "1" and "2", located at $\mathbf{0}$ and $a\hat{y}$, respectively. The unit reciprocal lattice vectors are thus given as $\vec{b}_1 = \frac{4\pi}{2\sqrt{3}a}\left(\hat{x} + \frac{1}{\sqrt{3}}\hat{y}\right)$ and $\vec{b}_2 = \frac{4\pi}{3a}\hat{y}$.

In the non-interacting limit with $\lambda = 0$, the Hamiltonian H can be expressed simply by the following tight-binding Hamiltonian

$$H_t = \sum_{\mathbf{k}}\sum_{\alpha,\beta}\sum_{i,j}\sum_{\sigma} H_{\alpha_i\beta_j}(\mathbf{k})c^\dagger_{\alpha_i\sigma}(\mathbf{k})c_{\beta_j\sigma}(\mathbf{k}), \tag{11}$$

where $c^\dagger_{\alpha_i\sigma}(\mathbf{k})$ is the Fourier transformation of the creation operator of an electron with orbital α and apin σ at the i-th basis site ($i = 1, 2$). The Hamiltonian matrix $H(\mathbf{k})$ is given as

$$H(\mathbf{k}) = \begin{pmatrix} 0 & 0 & 0 & 0 & te^{i(k_1+k_2)} & t \\ 0 & 0 & 0 & te^{i(k_1+k_2)} & 0 & te^{ik_2} \\ 0 & 0 & 0 & t & te^{ik_2} & 0 \\ 0 & te^{-i(k_1+k_2)} & t & 0 & 0 & 0 \\ te^{-i(k_1+k_2)} & 0 & te^{-ik_2} & 0 & 0 & 0 \\ t & te^{-ik_2} & 0 & 0 & 0 & 0 \end{pmatrix} \tag{12}$$

in the basis of $(ZX_1, XY_1, YZ_1, ZX_2, XY_2, YZ_2)$ for wave number $\mathbf{k} = \frac{k_1}{2\pi}\vec{b}_1 + \frac{k_2}{2\pi}\vec{b}_2$ with k_1 and k_2 being real numbers.

Introducing the (3×3) matrix

$$A(\mathbf{k}) = \begin{pmatrix} 0 & te^{i(k_1+k_2)} & t \\ te^{i(k_1+k_2)} & 0 & te^{ik_2} \\ t & te^{ik_2} & 0 \end{pmatrix}, \tag{13}$$

the Hamiltonian matrix $H(\mathbf{k})$ is expressed as

$$H(\mathbf{k}) = \begin{pmatrix} 0 & A(\mathbf{k}) \\ A(\mathbf{k})^\dagger & 0 \end{pmatrix}. \tag{14}$$

Let the eigenvalue and the eigenstate of $H(\mathbf{k})$ be E and $\mathbf{X}_E = \begin{pmatrix} X & Y \end{pmatrix}^{\mathrm{T}}$, respectively. Because

$$\begin{pmatrix} 0 & A(\mathbf{k}) \\ A(\mathbf{k})^\dagger & 0 \end{pmatrix} \begin{pmatrix} X \\ Y \end{pmatrix} = E \begin{pmatrix} X \\ Y \end{pmatrix}, \tag{15}$$

$A(\mathbf{k})Y = EX$ and $A(\mathbf{k})^\dagger X = EY$. We can thus rewrite the eigenvalue problem as

$$A(\mathbf{k})A(\mathbf{k})^\dagger X = t^2 \begin{pmatrix} 2 & e^{-ik_2} & e^{ik_1} \\ e^{ik_2} & 2 & e^{i(k_1+k_2)} \\ e^{-ik_1} & e^{-i(k_1+k_2)} & 2 \end{pmatrix} X = E^2 X. \tag{16}$$

By solving the above equation, we can obtain the following eigenstates

$$X_1^{\mathrm{T}} = \left(1,\ e^{ik_2},\ e^{-ik_1}\right), \tag{17}$$

$$X_2^{\mathrm{T}} = \left(0,\ e^{ik_2},\ -e^{-ik_1}\right), \tag{18}$$

$$X_3^{\mathrm{T}} = \left(-2,\ e^{ik_2},\ e^{-ik_1}\right), \tag{19}$$

whose eigenvalues are $4t^2$, t^2, and t^2, respectively. Since $Y = \frac{1}{E}A(\mathbf{k})^\dagger X$, we finally obtain the six eigenstates of $H(\mathbf{k})$ as

$$\mathbf{X}_{a_{1g}}(\mathbf{k}) = \frac{1}{\sqrt{6}}\left(1,\ e^{ik_2},\ e^{-ik_1},\ e^{-ik_1},\ e^{-i(k_1+k_2)},\ 1\right)^{\mathrm{T}}, \tag{20}$$

$$\mathbf{X}_{e_{2u,1}}(\mathbf{k}) = \frac{1}{2}\left(0,\ e^{ik_2},\ -e^{-ik_1},\ 0,\ -e^{-i(k_1+k_2)},\ 1\right)^{\mathrm{T}}, \tag{21}$$

$$\mathbf{X}_{e_{2u,2}}(\mathbf{k}) = \frac{1}{2\sqrt{3}}\left(-2,\ e^{ik_2},\ e^{-ik_1},\ 2e^{-ik_1},\ -e^{-i(k_1+k_2)},\ -1\right)^{\mathrm{T}}, \tag{22}$$

$$\mathbf{X}_{e_{1g,1}}(\mathbf{k}) = \frac{1}{2}\left(0,\ e^{ik_2},\ -e^{-ik_1},\ 0,\ e^{-i(k_1+k_2)},\ -1\right)^{\mathrm{T}}, \tag{23}$$

$$\mathbf{X}_{e_{1g,2}}(\mathbf{k}) = \frac{1}{2\sqrt{3}}\left(-2,\ e^{ik_2},\ e^{-ik_1},\ -2e^{-ik_1},\ e^{-i(k_1+k_2)},\ 1\right)^{\mathrm{T}}, \tag{24}$$

$$\mathbf{X}_{b_{1u}}(\mathbf{k}) = \frac{1}{\sqrt{6}}\left(1,\ e^{ik_2},\ e^{-ik_1},\ -e^{-ik_1},\ -e^{-i(k_1+k_2)},\ -1\right)^{\mathrm{T}}, \tag{25}$$

with the eigenvalues being $2t$, t, t, $-t$, $-t$, and $-2t$, respectively. Because all eigenvalues are wave number independent, we can call these energy bands as quasimolecular bands formed by quasimolecular orbitals (QMOs) with their symmetries, a_{1g}, e_{2u}, e_{1g}, and b_{1u}, indicated in the above eigenstates.

CLUSTER CALCULATIONS

To explore the correlation effect, we consider a periodic six-site cluster shown in Fig S1, which contains six holes for t_{2g}^5 systems. We take into account all states to represent the whole Hilbert space and thus the size of the Hilbert space is ${}_{36}C_6 = 1947792$. To solve Eq. (1) and find the ground state, we employ the exact diagonalization method based on Lanczos algorithm with the Jacobi preconditioner [S1]. We obtain the ground state and the corresponding eigenenergy with the energy accuracy of $4 \times 10^{-10}t$.

Hole density of a_{1g} band

Since only the a_{1g} band is fully empty in the non-relativistic and non-interacting limits for t_{2g}^5 systems, the hole density in the a_{1g} quasimolecular band is a good quantity to quantify how far the ground state is from the pure QMO state. The hole density operator $\bar{\rho}_{a_{1g}}(\mathbf{k})$ per site at the wave number $\mathbf{k}$ is defined as

$$\bar{\rho}_{a_{1g}}(\mathbf{k}) = \frac{1}{2}\sum_\sigma c_{a_{1g}\sigma}(\mathbf{k})c^\dagger_{a_{1g}\sigma}(\mathbf{k}), \tag{26}$$

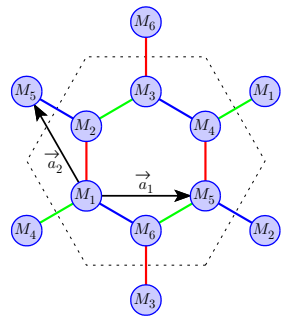

FIG. S1. Schematic diagram of a periodic six-site cluster (containing $M_1, M_2, \ldots,$ and M_6 sites) indicated by dashed line surrounding the cluster. Red, green, and blue bonds represent the XY-, YZ-, and ZX-directions, respectively (see table S1). The unit lattice vectors $\vec{a}_1 = \sqrt{3}a\hat{x}$ and $\vec{a}_2 = -\frac{\sqrt{3}a}{2}\hat{x} + \frac{3a}{2}\hat{y}$ of the honeycomb lattice are also indicated.

where the creation operator $c^\dagger_{a_{1g}\sigma}(\mathbf{k})$ is the eigenstate of $H(\mathbf{k})$ and is given as $c^\dagger_{a_{1g}\sigma}(\mathbf{k}) = \sum_{j,\nu}[\mathbf{X}_{a_{1g}}(\mathbf{k})]_{\nu_j} c^\dagger_{\nu_j\sigma}(\mathbf{k})$. Here $[\mathbf{X}_{a_{1g}}(\mathbf{k})]_{\nu_j}$ ($j = 1, 2$ and $\nu = ZX, XY, YZ$) is the ν_j-th element of the eigenstate of $H(\mathbf{k})$ with a_{1g} symmetry given in Eq. (20). For the six-site cluster with periodic boundary conditions, there exist three independent wave numbers, i.e., $(k_1, k_2) = (0, 0)$ (Γ point), $(\frac{\pi}{3}, \frac{\pi}{3})$ (K point), and $(\frac{2\pi}{3}, \frac{2\pi}{3})$ (K' point), and $c^\dagger_{a_{1g}\sigma}(\mathbf{k})$ for these wave numbers are expressed as

$$c^\dagger_{a_{1g}\sigma}(\mathbf{k}) = \frac{1}{\sqrt{3}}\Big(\sum_\nu [\mathbf{X}_{a_{1g}}(\mathbf{k})]_{\nu_1} c^\dagger_{1\nu\sigma} + \sum_\nu [\mathbf{X}_{a_{1g}}(\mathbf{k})]_{\nu_2} c^\dagger_{2\nu\sigma} + \sum_\nu [\mathbf{X}_{a_{1g}}(\mathbf{k})]_{\nu_1} e^{-i(k_1+k_2)} c^\dagger_{3\nu\sigma} + \sum_\nu [\mathbf{X}_{a_{1g}}(\mathbf{k})]_{\nu_2} e^{-ik_1} c^\dagger_{4\nu\sigma} + \sum_\nu [\mathbf{X}_{a_{1g}}(\mathbf{k})]_{\nu_1} e^{-ik_1} c^\dagger_{5\nu\sigma} + \sum_\nu [\mathbf{X}_{a_{1g}}(\mathbf{k})]_{\nu_2} e^{ik_2} c^\dagger_{6\nu\sigma}\Big), \tag{27}$$

where $c^\dagger_{j\nu\sigma}$ is the creation operator of an electron with orbital $\nu = (YZ, ZX, XY)$ and spin $\sigma = (\uparrow, \downarrow)$ at site M_j in the six-site cluster shown in Fig. S1. In the main text, we calculate the hole density at the Γ point, i.e.,

$$\bar{n}_{a_{1g}} = \langle \Psi_0 | \bar{\rho}_{a_{1g}}(\mathbf{k} = 0) | \Psi_0 \rangle, \tag{28}$$

where $|\Psi_0\rangle$ is the ground state of the six-site cluster. This quantity $\bar{n}_{a_{1g}}$ is exactly one for the pure QMO state.

Doublon-holon excitations in $j_{\rm eff} = 1/2$ orbitals

To explore the distribution of a doublon-holon pair in the $j_{\rm eff} = 1/2$ orbitals at neighboring sites, we calculate the projected spectrum

$$\begin{aligned}\Lambda_{1/2}(\omega) &= \sum_n \sum_{s_3,s_4,s_5,s_6} |\langle D_{s_3,s_4,s_5,s_6} | \Psi_n \rangle|^2 \, \delta(\omega - E_n + E_0) \\ &= -\frac{1}{\pi} \mathrm{Im} \sum_{s_3,s_4,s_5,s_6} \langle D_{s_3,s_4,s_5,s_6} | \frac{1}{\omega - H + E_0 + i\delta} | D_{s_3,s_4,s_5,s_6} \rangle,\end{aligned} \tag{29}$$

where $|\Psi_n\rangle$ and E_n are the n-th eigenstate and eigenvalue of H, respectively, and the ground state corresponds to $n = 0$. $|D_{s_3,s_4,s_5,s_6}\rangle$ is a single doublon-holon pair excited state in the NN $j_{\rm eff} = 1/2$ orbitals at sites M_1 and M_2 (see Fig. S1), defined as

$$|D_{s_3,s_4,s_5,s_6}\rangle = d_{1,+1/2} d_{1,-1/2} d_{3,s_3} d_{4,s_4} d_{5,s_3} d_{6,s_6} |\mathrm{FO}\rangle, \tag{30}$$

where $|\mathrm{FO}\rangle$ is the fully occupied state with electrons and d_{l,s_l} is the annihilation operator of $j_{\rm eff} = 1/2$ electron with isospin s_l ($= \pm 1/2$) [given in Eqs. (5) and (6)] at site M_l in the six-site cluster shown in Fig. S1. To calcuate $\Lambda_{1/2}(\omega)$, we employ the continued faction method [S2]. We perform 500 iterations of the continued faction with $\delta = 0.12t$.

As shown in Figs. 4(a)–(c) of the main text, the U dependence of the low-energy peak positions in $\Lambda_{1/2}(\omega)$ for given λ is qualitatively different in the two insulators, i.e., the quasimolecular band insulator and the relativistic Mott insulator. As shown in Fig. S2, the similar change of behavior is found even when λ is varied for fixed U and

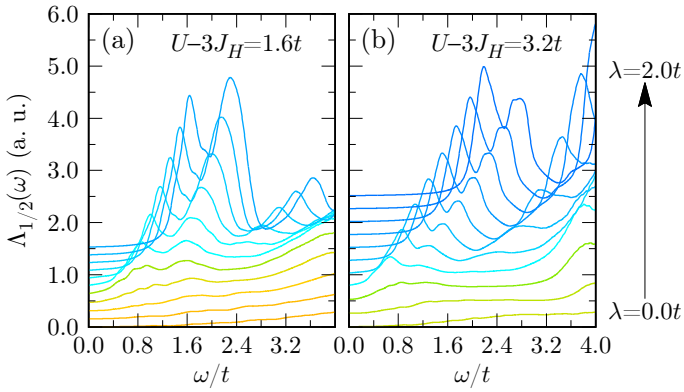

FIG. S2. (Color online) Doublon-holon excitation spectrum $\Lambda_{1/2}(\omega)$ for (a) $U - 3J_{\rm H} = 1.6t$ and (b) $3.2t$ with varying λ indicated in the figure. Here we set $J_{\rm H} = 1.6t$ and different line colors correspond to the values of $\bar{n}_{a_{1g}}$ shown in Fig. 3(b) of the main text.

$J_{\rm H}$. With increasing λ, the low-energy peak positions first shift downward in energy and then move upward once we cross the crossover region. The increase of the low-energy peak positions supports that the edge of $\Lambda_{1/2}(\omega)$ in the relativistic Mott limit is evidently coupled with the local d-d excitation, whose excitation energy is proportional to λ. Therefore, the exciton-like peak as well as the spin-orbit exciton peak in the RIXS spectrum should also shift upward with increasing λ. The decrease of the low-energy peak positions in $\Lambda_{1/2}(\omega)$ in the QMO limit is due to the decrease of a band gap with increasing λ, as shown in Fig. 2(b) of the main text.

Optical conductivity

To calculate the optical conductivity (OC), we adopt the Kubo formula

$$\begin{aligned}\sigma(\omega) &= \frac{\pi v}{\omega}\sum_{n(\neq 0)} |\langle\Psi_n|\hat{J}_c|\Psi_0\rangle|^2\delta(\omega - E_n + E_0)\\ &= -v\ \mathrm{Im}\sum_{n(\neq 0)}\frac{|\langle\Psi_n|\hat{J}_c|\Psi_0\rangle|^2}{(E_n - E_0)(\omega - E_n + E_0 + i\delta)}\\ &= -v\ \mathrm{Im}\Big[\frac{1}{\omega + i\delta}\sum_{n(\neq 0)}\Big(\frac{|\langle\Psi_n|\hat{J}_c|\Psi_0\rangle|^2}{E_n - E_0} + \frac{|\langle\Psi_n|\hat{J}_c|\Psi_0\rangle|^2}{\omega - E_n + E_0 + i\delta}\Big)\Big]\\ &= -v\ \mathrm{Im}\Big[\frac{1}{\omega + i\delta}\Big(\langle\Psi_0|\hat{J}_c\frac{1}{H - E_0}\hat{J}_c|\Psi_0\rangle + \langle\Psi_0|\hat{J}_c\frac{1}{\omega - H + E_0 + i\delta}\hat{J}_c|\Psi_0\rangle\Big)\Big],\end{aligned} \tag{31}$$

where v is the volume per site and $\hat{J}_c$ is the current operator along the XY-direction given as

$$\hat{J}_c = -\frac{ie}{A\hbar}\sum_{\mu,\nu,\sigma}\big(t^{XY}_{\mu\nu}c^\dagger_{2\nu\sigma}c_{1\mu\sigma} - t^{XY}_{\mu\nu}c^\dagger_{1\mu\sigma}c_{2\nu\sigma}\big), \tag{32}$$

where $e\,(<0)$ is the electronic charge and A is the area facing neighboring sites. Note that the OCs for the YZ- and ZX-directions are exactly the same as that for the XY-direction because of the symmetry. We employ the continued fraction method to calculate the spectrum in Eq. (31). We perform 400 iterations of the continued fraction with $\delta = 0.4t$.

Resonant inelastic x-ray scattering spectrum

To calculate the resonant inelastic x-ray scattering (RIXS) spectrum $I\,(\omega, \mathbf{q}, \epsilon, \epsilon')$, we follow the Kramers-Heisenberg formula, i.e.,

$$I\,(\omega, \mathbf{q}, \epsilon, \epsilon') = \sum_n |\mathcal{F}_{n0}(\omega, \mathbf{q}, \epsilon, \epsilon')|^2\delta\,(\omega - E_n + E_0)\,, \tag{33}$$

where $\omega = \omega_{\mathbf{k}} - \omega_{\mathbf{k}'}$ and $\mathbf{q} = \mathbf{k} - \mathbf{k}'$ when an incident (outgoing) x-ray has momentum $\mathbf{k}$ ($\mathbf{k}'$), energy $\omega_{\mathbf{k}}$ ($\omega_{\mathbf{k}'}$), and polarization ϵ (ϵ') [S3]. Adopting the dipole and fast collision approximations, $\mathcal{F}_{n0}(\omega, \mathbf{q}, \epsilon, \epsilon')$ is described as $\mathcal{F}_{n0}(\omega, \mathbf{q}, \epsilon, \epsilon') = \frac{1}{i\Gamma}\langle\Psi_n|R(\epsilon', \epsilon, \mathbf{q})|\Psi_0\rangle$, where Γ is a lifetime broadening for the intermediate states. The RIXS scattering operator $R(\epsilon', \epsilon, \mathbf{q})$ is given as

$$R(\epsilon', \epsilon, \mathbf{q}) = \sum_i \sum_{\nu,\nu',\sigma} e^{i\mathbf{q}\cdot\mathbf{r}_i} T_{\nu'\nu}(\epsilon', \epsilon) c_{i\nu'\sigma} c^{\dagger}_{i\nu\sigma}, \tag{34}$$

where $T_{\nu'\nu}(\epsilon', \epsilon) = \sum_s \langle\phi_s|\epsilon' \cdot \mathbf{r}|\psi_{\nu'}\rangle\langle\psi_\nu|\epsilon \cdot \mathbf{r}|\phi_s\rangle$, $\mathbf{r}_i$ is the position vector of site i, ψ_ν is the local atomic wave function for t_{2g} orbital ν, and ϕ_s refers to the core-hole wave function ($2p_{3/2}$ for the L_3-edge spectrum). The RIXS spectrum $I(\omega, \mathbf{q}, \epsilon, \epsilon')$ is finally given as

$$I(\omega, \mathbf{q}, \epsilon, \epsilon') = -\frac{1}{\pi\Gamma}\mathrm{Im}\Big[\langle\Psi_0|R(\epsilon', \epsilon, \mathbf{q})\frac{1}{\omega - H + E_0 + i\delta}R(\epsilon', \epsilon, \mathbf{q})|\Psi_0\rangle\Big]. \tag{35}$$

For the calculations in the main text, we set $\epsilon = \frac{1}{\sqrt{2}}\hat{x} + \frac{1}{\sqrt{2}}\hat{z}$, $\epsilon' = \hat{y}$, and $\mathbf{q} = 0$ where the incident and outgoing x-rays have π and σ polarizations, respectively, with 45° scattering angles for the honeycomb plane. The geometry is in principle the same as the experimental setup in Ref. S4. We employ the continued fraction method to evaluate the RIXS spectrum and perform 300 iterations of the continued fraction with $\delta = 0.08t$.

LOCAL MULTIPLET STRUCTURE

It is instructive to examine the energy hierarchy of local multiplets, which is obtained simply by solving the single-site terms in Eq. (1). Figure S3 summarizes the energy hierarchy of three relevant configurations, i.e., d^4, d^5, and d^6 electron configurations in the t_{2g} manifold.

In the case of d^5 electron configuration, only the SOC plays a role in determining the doublet ($J_{\mathrm{eff}} = 1/2$) and quartet ($J_{\mathrm{eff}} = 3/2$) states with their energies $E_0 - \lambda$ and $E_0 + \frac{\lambda}{2}$, respectively, while the Hund's coupling J_{H} cannot have any effect on their multiplets. Here, E_0 is the energy for d^5 electron configuration when $\lambda = 0$. Because the energy splitting between these two manifolds is $\frac{3}{2}\lambda$, the local d-d transition, which is accessed by the RIXS spectrum, appears in this energy region.

On the contrary, in the case of d^4 electron configuration, not only λ but also J_{H} determines the multiplet hierarchy. When $J_{\mathrm{H}} \neq 0$ but $\lambda = 0$, fifteen-fold degenerate states split into nine-fold degenerate states with total angular moment $L = 1$ and total spin momentum $S = 1$, five-fold degenerate states with $L = 2$ and $S = 0$, and a single state with $L = S = 0$. Their energies are, respectively, $E_0 - 4U + 7J_{\mathrm{H}}$, $E_0 - 4U + 9J_{\mathrm{H}}$, and $E_0 - 4U + 12J_{\mathrm{H}}$, thus following

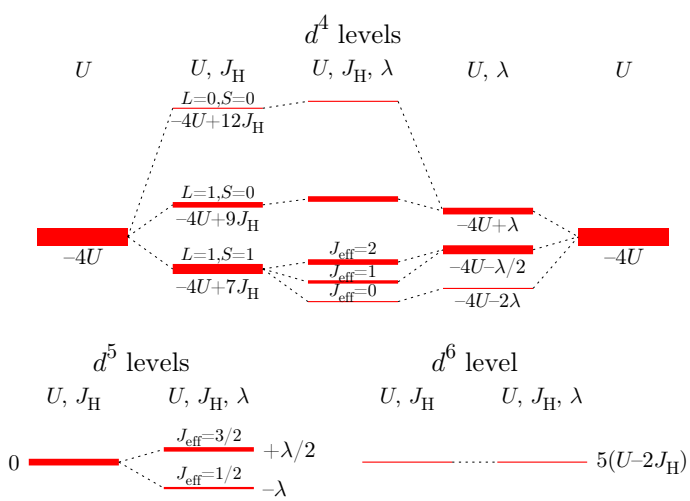

FIG. S3. (Color online) Schematic energy diagrams of multiplet hierarchy in the atomic limit for three relevant electron configurations, i.e., d^4, d^5, and d^6 in the t_{2g} manifold. The multiplet energy levels are represented by red lines (the width is proportional to the degeneracy) when non-zero U, J_{H}, or/and λ (indicated at the top of each diagram) are considered. The multiplet energy shown in each level is measured from the d^5 multiplet energy E_0 without the SOC.

the Hund's rule. A finite λ induces addition splittings. The lowest nine-fold degenerate states are split into $J_{\rm eff}=0$, $J_{\rm eff}=1$, and $J_{\rm eff}=2$ states. Because there are non-negligible mixing between the $J_{\rm eff}=0$ state and the singlet state with $L=S=0$, and also between the $J_{\rm eff}=2$ states and the five-fold degenerate states with $L=2$ and $S=0$, the exact energy levels for the $J_{\rm eff}=0$ and $J_{\rm eff}=2$ states are not simply expressed analytically. However, the energy difference between the $J_{\rm eff}=0$ and $J_{\rm eff}=2$ states is always $\frac{3}{2}\lambda$. The energy of the $J_{\rm eff}=1$ states is instead given analytically as $E_0-4U+7J_{\rm H}-\frac{\lambda}{2}$. When $J_{\rm H}\gg\lambda$, the energies of the $J_{\rm eff}=0$ and $J_{\rm eff}=2$ states are obtained as $E_0-4U+7J_{\rm H}-\lambda$ and $E_0-4U+7J_{\rm H}+\frac{\lambda}{2}$, respectively. In the opposite limit $\lambda\gg J_{\rm H}$, their energies are given as $E_0-4U+7J_{\rm H}-2\lambda$ and $E_0-4U+7J_{\rm H}-\frac{\lambda}{2}$, respectively.

Note that the optical excitations are determined in the multiplet theory by the energy difference between the ground state in d^5d^5 electron configuration and the excited states in d^4d^6 electron configuration. Therefore, the lowest optical peak appears at $U-3J_{\rm H}$ when $\lambda=0$. When λ is finite, the lowest optical peaks are composed of three subpeaks. The central peak, which corresponds to the $J_{\rm eff}=1$ multiplet in the d^4 electron configuration, appears at $U-3J_{\rm H}+\frac{3\lambda}{2}$. The first (third) lowest peak, related to the $J_{\rm eff}=0$ ($J_{\rm eff}=2$) multiplet in the d^4 electron configuration, appears in an energy range between $U-3J_{\rm H}$ ($U-3J_{\rm H}+\frac{3\lambda}{2}$) and $U-3J_{\rm H}+\lambda$ ($U-3J_{\rm H}+\frac{5\lambda}{2}$), depending on the relative strength of $J_{\rm H}$ and λ. Since the hopping between the nearest neighboring $j_{\rm eff}=1/2$ orbitals is absent when the hopping is mediated via the edge-shared oxygens, the optical peak attributed to the $J_{\rm eff}=0$ multiplet in the d^4 electron configuration is diminished [S5]. Contribution of the third multiplet ($J_{\rm eff}=2$) in the d^4 electron configuration is also suppressed because its optical transition amplitude between $J_{\rm eff}=1/2$ in the d^5 electron configuration and $J_{\rm eff}=2$ in the d^4 electron configuration is as small as quarter of that between $J_{\rm eff}=1/2$ in the d^5 electron configuration and $J_{\rm eff}=1$ in the d^4 electron configuration. Therefore, the honeycomb lattice system in the relativistic Mott limit shows a dominant optical peak at $U-3J_{\rm H}+\frac{3\lambda}{2}$, attributed to the excitation to the $J_{\rm eff}=1$ multiplet in the d^4 electron configuration.

EFFECT OF DIRECT HOPPING t' BETWEEN NEIGHBORING d ORBITALS

Even thought the dominant hopping process in the honeycomb lattice structure is via the ligand p orbitals, the spatial extension of $4d$ and $5d$ orbitals is large enough to give rise to the direct hopping between neighboring transition metal d orbitals. Recent theoretical study based on first-principles density functional calculations has estimated that the direct hopping t' between XY, YZ, and ZX orbitals along the XY-, YZ-, and ZX-directions, respectively, can be as large as $t'/t\approx 0.10$ for Na_2IrO_3 and -0.97 for α-$RuCl_3$ [S6]. Therefore, t' is also an important parameter in determining the electronic state specially for α-$RuCl_3$.

Figure S4 presents the OC and RIXS spectra for various values of t' when $U-3J_{\rm H}=6t$, $J_{\rm H}=1.6t$, and $\lambda=0.8t$. An interesting feature is that the low-energy optical peaks arise around $2t$ in addition to the dominant peaks with the large spectral weight near $7t$. For small $|t'|$ ($\leq 0.4t$), the small low-energy optical peaks appear near the dominant RIXS peak ($\approx 1.4t$) and the higher edge of the RIXS spectra ($\approx 2.5t$), which is in good agreement with the experimental observations [S7, S8]. Notice that the dominant RIXS peak is attributed to the local d-d transition from the $j_{\rm eff}=3/2$ to $1/2$ orbitals. The direct hopping t' enhances the optical contribution of the electron-hole excitation between the neighboring $j_{\rm eff}=1/2$ orbitals, largely suppressed in the edge-shared geometry without t'. Our results thus imply that the unusual coupling between these two different types of excitations, i.e., the electron-hole excitations between the neighboring $j_{\rm eff}=1/2$ orbitals and the local d-d excitations, can play a role in the low-energy optical excitations. It should be noted here that the coupling is possible because of the finite inter-band hopping between the $j_{\rm eff}=1/2$ and $3/2$ bands [S5].

For large $|t'|$ ($\geq 0.6t$), we find in Fig. S4 that a large amount of spectral weights in the OC are transferred from the high-energy region ($\gtrsim 4t$) to the low-energy region ($\lesssim 4t$). This observation with a large amount of low-energy spectral weight is far from the experimental observations [S7, S8] and thus indicates that the density functional calculations overestimate $|t'|$.

[S1] R. B. Morgan and D. S. Scott, SIAM J. Sci. Comput. **14**, 585 (1993).
[S2] E. Dagotto, Rev. Mod. Phys. **66**, 763 (1994).
[S3] L. J. P. Ament, M. van Veenendaal, T. P. Devereaux, J. P. Hill, and J. van den Brink, Rev. Mod. Phys. **83**, 705 (2011).
[S4] S. H. Chun, J.-W. Kim, J. Kim, H. Zheng, C. C. Stoumpos, C. D. Malliakas, J. F. Mitchell, K. Mehlawat, Y. Singh, Y.

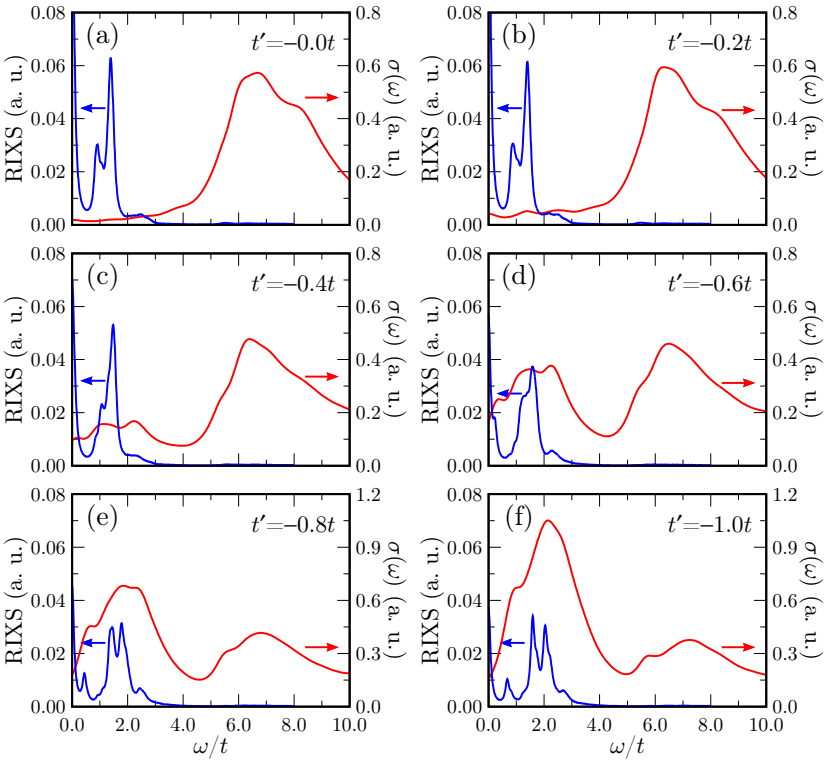

FIG. S4. (Color online) OC $\sigma(\omega)$ (red lines) and L_3-edge RIXS spectrum (blue lines) for various direct d-d hoppings t' indicated in the figures for $U - 3J_{\rm H} = 6t$, $J_{\rm H} = 1.6t$, and $\lambda = 0.8t$.

Choi, T. Gog, A. Al-Zein, M. M. Sala, M. Krisch, J. Chaloupka, G. Jackeli, G. Khaliullin, and B. J. Kim, Nature Phys. **11**, 462 (2015).

[S5] B. H. Kim, G. Khaliullin, and B. I. Min, Phys. Rev. B **89**, 081109(R) (2014).

[S6] S. M. Winter, Y. Li, H. O. Jeschke, and R. Valentí, arXiv:1603.02548.

[S7] K. W. Plumb, J. P. Clancy, L. J. Sandilands, V. V. Shankar, Y. F. Hu, K. S. Burch, H.-Y. Kee, and Y.-J. Kim, Phys. Rev. B **90**, 041112(R) (2014).

[S8] L. J. Sandilands, Y. Tian, A. A. Reijnders, H.-S. Kim, K. W. Plumb, Y.-J. Kim, H.-Y. Kee, and K. S. Burch, Phys. Rev. B **93**, 075144 (2016).